THE JOURNAL OF PHYSICAL CHEMISTRY C

Article

pubs.acs.org/JPCC

Surface-Enhanced Hyper-Raman Scattering: A New Road to the Observation of Low Energy Molecular Vibrations

Jérémy Butet* and Olivier J. F. Martin

Nanophotonics and Metrology Laboratory (NAM), Swiss Federal Institute of Technology Lausanne (EPFL), 1015, Lausanne, Switzerland

Supporting Information

ABSTRACT: The plasmon enhancement of molecular hyper-Raman scattering, the nonlinear counterpart of Raman scattering, which involves the absorption of two fundamental photons, is investigated with emphasis on low energy molecular vibrations. The two-photon excitation of the molecule is treated using its hyperpolarizability β, and the emission of the hyper-Raman photons is computed using a dipole emitter located at the molecule position. The electromagnetic response of the plasmonic systems is evaluated using a surface integral equation method, which makes possible considering both planewave and dipole excitations in a single formalism. Taking into account different geometries (including multiresonant antennas and silver heptamers supporting Fano resonances), the experimental parameters influencing the enhancement of the molecular hyper-Raman scattering are discussed in detail. In particular, it is shown that a good excitation at the fundamental stage is not sufficient for reaching a good enhancement factor and that an optimization of the electromagnetic response of the plasmonic substrate is also important at the emission wavelength. The competition between the molecular hyper-Raman scattering signal and the background signal, that is, the second harmonic generation, is discussed. The latter can be reduced in specific structures by taking advantages of the key role played by the symmetry of the structure for hyper-Raman scattering and second harmonic generation. This way, we propose a nanostructure where the second harmonic generation can be reduced in the detection direction, enabling the hyper-Raman scattering signal from single donor−acceptor "push−pull" chromophores to be experimentally recorded with a low noise level using surface-enhanced hyper-Raman scattering. It is particularly remarkable that the hyper-Raman signal from one molecule can be stronger than the second harmonic generation from a complete plasmonic nanostructure, despite the considerable volume difference between both nano-objects. This fundamental observation stems from the different selection rules for both nonlinear optical processes.

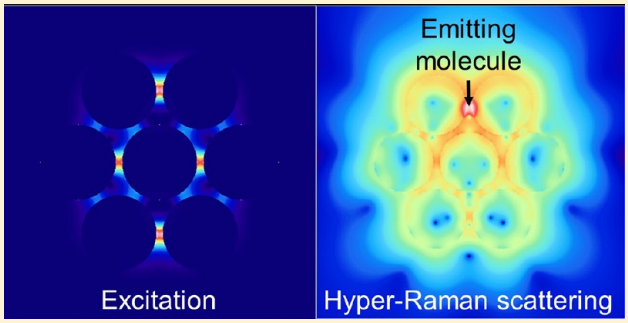

INTRODUCTION

Recording the optical response of molecules is a fundamental method for measuring their vibrational and chemical properties.[1] However, some of the information is lost in ensemble measurements because only averaged values are accessible. As a consequence, the most subtle physical phenomena occurring in molecules cannot be observed in ensemble measurements and single molecule measurements are necessary for their full understanding.[2,3] The observation of energy transfer in a single light-harvesting complex is a good example of the recent achievements in this field of research.[4] However, the interaction between an optical field and a single molecule is very weak, and plasmonic nanoantennas have proved themselves as a helping hand for the observation of single molecules.[5−8] Indeed, plasmonic nanostructures have the ability to concentrate incoming light into a tiny volume, down to the nanoscale, and to control the emission of a molecule located in its vicinity, thus opening the way for surface-enhanced spectroscopy techniques.[9−13] Among all of the surface-enhanced spectroscopy techniques, the most popular and used is indubitably surface-enhanced Raman spectroscopy (SERS).[14−20] Raman scattering (RS) is a spectroscopy technique that measures the vibrational modes of a given molecule. In a first approximation, one can consider that the enhancement of the Raman intensity scales with the fourth power of the local electric field, emphasizing the benefit of localized surface plasmon resonances for its observation.[8,14−21] The high local electric field provided by plasmonic nanostructures has also been used to increase the infrared absorption of molecules (surface-enhanced infrared spectroscopy),[13,22,23] as well as coherent anti-Stokes Raman spectroscopy.[24−26] Coherent anti-Stokes Raman spectroscopy has been recently used to follow, in real time, the vibration of a single molecule sandwiched by two gold nanoparticles. In this time-resolved experiment, the main challenge was to separate the coherent anti-Stokes Raman spectroscopy signal from the single molecule and the strong

Received: April 30, 2015
Revised: June 9, 2015
Published: June 10, 2015

DOI: 10.1021/acs.jpcc.5b04128
J. Phys. Chem. C 2015, 119, 15547−15556

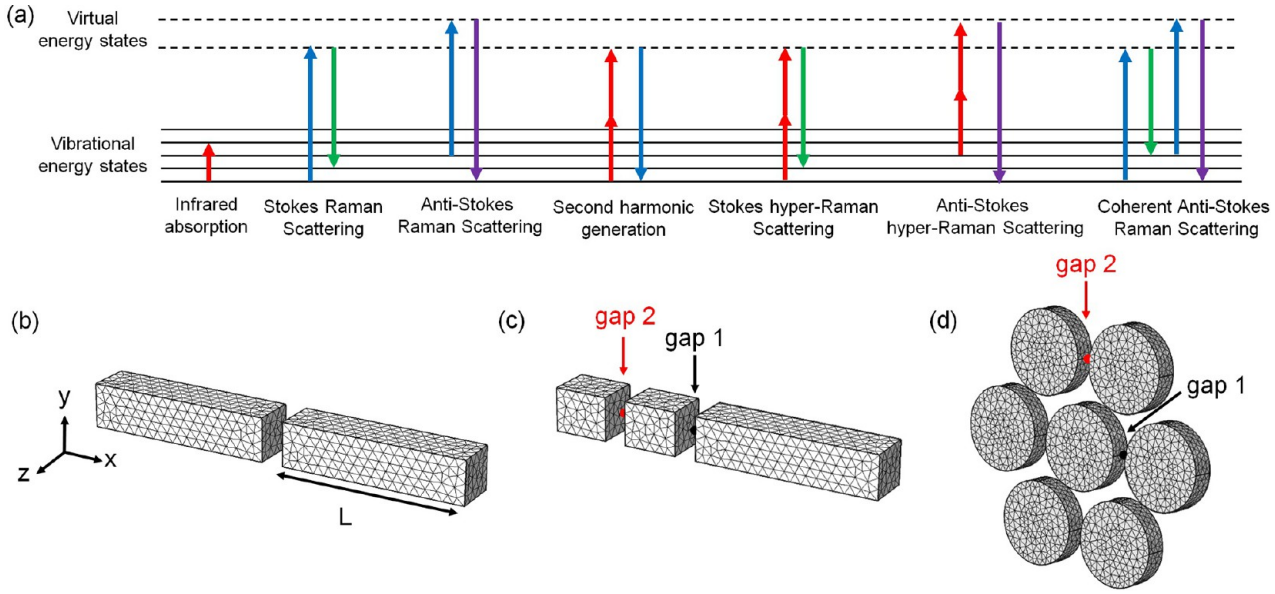

Figure 1. (a) Jablonski diagram illustrating the different spectroscopy techniques discussed in this Article. Geometries of the plasmonic nanostructures studied in this Article with the corresponding meshes used for the numerical computations: (b) aluminum dipolar nanoantennas, (c) double resonant antenna (DRA) made with aluminum, and (d) silver heptamers. The length of the dipolar nanoantennas arms varies from L = 110 to 190 nm. The width and height are fixed to 40 nm and the nanogap to 20 nm. For the DRA, the length of the small bars is 40 nm and the length of the long bar is 170 nm. For the silver heptamers, the nanoparticle diameter varies from 70 to 120 nm. The height is fixed to 30 nm and the interparticle distance to 10 nm. The arrows indicate the gaps mentioned in the main text and the other figures.

coherent anti-Stokes Raman spectroscopy signal from the gold nanodimer itself.[27] In this Article, we turn attention to hyper-Raman scattering (HRS), which is another nonlinear optical phenomenon to probe molecular vibrations but involving only two pump photons contrary to coherent anti-Stokes Raman spectroscopy, which involves an additional Stokes photon; see Figure 1a. Contrary to its linear counterpart, the enhancement of HRS has only been sparsely studied despite its clear potential for the observation of low energy molecular vibrations and vibrational molecular modes inactive in both RS and infrared absorption.[28−31] Contrary to RS, HRS involves the absorption of two fundamental photons, and, consequently, the HRS is well separated spectrally from the incident laser light, which represents a significant experimental advantage; see Figure 1a.[28−31] Indeed, the rejection of the laser light is an important problem for the observation of low energy molecular vibrations with SERS because the spectral shift from the laser wavelength is small for this inelastic optical process. Furthermore, HRS is a nonlinear optical process, which involves three photons in total and must obey specific selection rules.[32] These selection rules were theoretically derived in the framework of the group theory demonstrating that some of the vibrational molecular modes active in HRS are inactive in both RS and infrared absorption.[32] It is then obvious that HRS is complementary to both RS and infrared absorption, which are nowadays well-known and established spectroscopy techniques. Unfortunately, the specific molecular information provided by HRS cannot be exploited without any plasmon enhancement, because the HRS signal from a single molecule is several orders of magnitude weaker than the RS signal.[28] For example, the ratio between HRS and RS has been estimated to be 5×10^{-9} for bulk crystal violet molecules at a laser power of 10^7 W/cm^2.[33−35] However, the important criteria for making a good plasmonic substrate for surface-enhanced hyper-Raman scattering (SEHRS) have not been discussed in detail as was done in the past for SERS and SIERA.[36,37] The development of such an efficient substrate can unleash the potential of SEHRS, down to the single molecule sensitivity.[38]

In this Article, we numerically study the design and the optimization of plasmonic substrates for SEHRS. Following an approach previously developed for the study of SERS,[39] the two-photon excitation of the molecule is treated using its hyperpolarizability β, and the electromagnetic response of the plasmonic systems is computed with a surface integral equation (SIE) method.[40,41] Taking into account different geometries (including multiresonant antennas[42] and Fano resonant oligomers[43]), the different parameters influencing the HRS enhancement are discussed. Because HRS is a tool of choice for recording low energy molecular vibrations, we also discuss how the background signal, that is, the SHG, can be reduced in the detection direction and demonstrate that the HRS signal from single donor−acceptor "push−pull" chromophores can be experimentally recorded with a low noise level using SEHRS.

NUMERICAL METHODS

The linear optical responses have been calculated using a surface integral formulation.[40,41] All of the nanostructures are embedded in a homogeneous medium with refractive index n = 1.25 reproducing the influence of a glass substrate on their optical response. The dielectric constants for gold are taken from experimental data at both the fundamental and the second harmonic wavelengths.[44] For the SHG computations, the linear surface currents are used for the evaluation of the fundamental electric fields just below the gold surfaces and then used for the calculation of the surface second harmonic polarization.[45,46] Only the component $\chi_{surf,nnn}$ of the surface tensor, where "n" denotes the component normal to the surface, is considered. Recent experimental results shows that this term dominates the surface response of metallic nanoparticles.[47,48] Note that other contributions to the second harmonic signal, the component

DOI: 10.1021/acs.jpcc.5b04128
J. Phys. Chem. C 2015, 119, 15547−15556

$\chi_{surf,ttn}$ of the surface tensor (where t denotes the component tangential to the surface) and bulk contribution, are theoretically allowed, but these terms contribute only weakly to the total second harmonic wave.[47,48] The second harmonic surface currents are obtained solving the SIE formulation taking into account the nonlinear polarization and enforcing the boundary conditions at the nanostructure surfaces.[49] As the linear surface currents, the second harmonic surface currents are expanded on RWG basis functions. The expanding coefficients are found applying the method of moments with Galerkin's testing.[40,41] A Poggio–Miller–Chang–Harrington–Wu formulation is used to ensure accurate solutions even at resonant conditions.[40,41] The second harmonic electric field is then deduced from the second harmonic surface currents using a two-term subtraction method for the evaluation of Green's functions.[45,46]

RESULTS AND DISCUSSION

The nanostructures investigated in this Article are shown in Figure 1. Aluminum dipolar antennas (DA) with various arm lengths L (ranging from 110 to 190 nm) are first considered, Figure 1b. These structures exhibit a single resonance. Next, we discuss nanostructures specifically designed to exhibit spectral features at both the fundamental and the second harmonic wavelengths: double resonant antennas (DRA, Figure 1c) and silver heptamers, Figure 1d. Because we are interested in nonlinear phenomena in the short wavelength range of the visible spectrum, we resort to aluminum (Al) for the different nanostructures investigated here; indeed, Al is much better suited than gold or silver for that part of the spectrum. The dispersive permittivity values for Al are taken from the scientific literature.[50]

Let us first evaluate the electromagnetic responses of Al dipolar nanoantennas using the SIE method.[41] The intensity enhancement at the gap center, defined as the intensity at the gap center divided by the intensity of the incoming wave, is shown as a function of the wavelength of the incident wave for different antenna lengths L in Figure 2a. A planewave polarized along the x-direction and propagating along the z-direction is considered. As expected, the resonance wavelength red-shifts when the antenna length increases. In the following, a pump with a wavelength λ = 800 nm will be considered for the evaluation of the SEHRS signal; note however that the present study can be extended to any pump wavelength without any difficulties. In this configuration, the highest intensity enhancement is obtained for L = 150 nm. The radiative properties of a dipole emitter are also modified by a plasmonic system in its vicinity.[51−56] The influence of the Al DA on the enhancement of a dipole source located at the gap center and aligned along the x-axis is now calculated. Figure 2a shows the emitted intensity evaluated in the far-field region, at the point (0, 0, 50 μm), normalized to the emitted intensity for an isolated dipole in a homogeneous medium without DA. The result is identical to the intensity enhancement in the nanogap when the nanoantennas are driven by an incoming planewave, as expected from reciprocity.[40] As we will see in the following, the determination of the HRS enhancement is straightforward using the reciprocity between far-field excitation and dipole emission.[57]

Having determined the electromagnetic properties of the Al DA, we now turn our attention to the SEHRS. The HRS intensity from a molecule is related to its hyperpolarizability β. Note that an alternative excitation mechanism, involving SHG

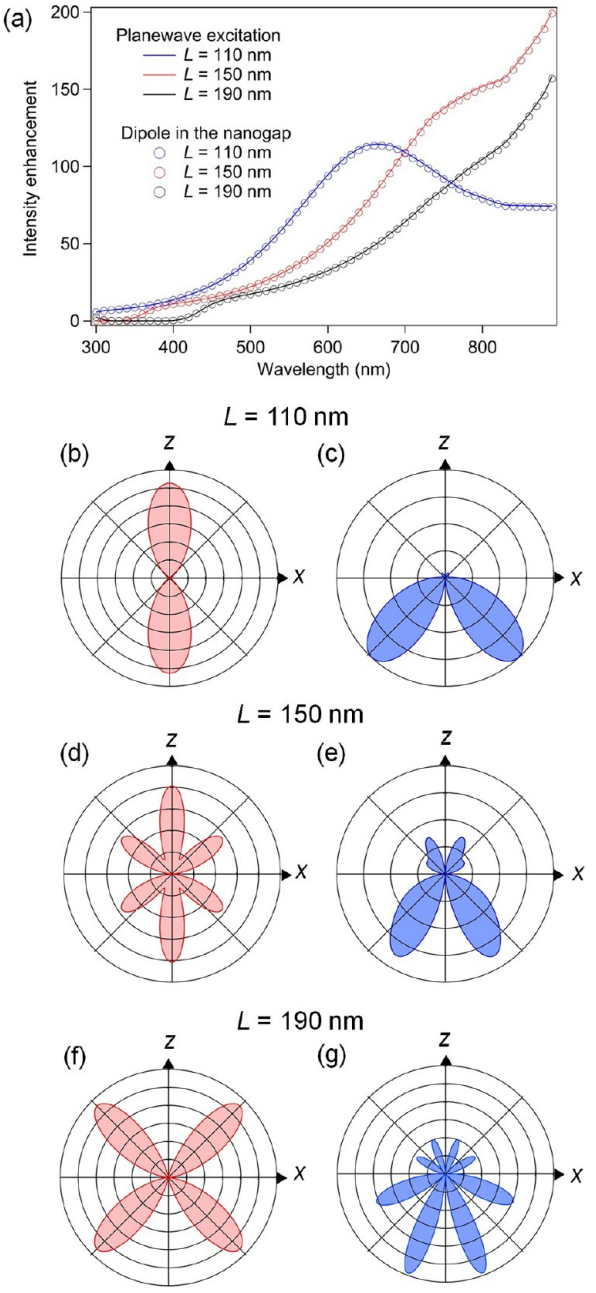

Figure 2. (a) Enhancement of the intensity in the gap of Al dipolar nanoantennas (continuous lines) and enhancement of the radiation from a dipole located at the gap center and polarized along the x-axis (dot). In the latter case, the intensity is evaluated in the far-field region (at the point (0, 0, 50 μm)). The gap dimension is fixed at 20 nm, and the nanoantenna arm length is L = 110 nm (blue), 150 nm (red), and 190 nm (black). Emission patterns for a dipole located at the gap center (λ = 400 nm) for (b) L = 110 nm, (d) L = 150 nm, and (f) L = 190 nm. The emission patterns of the SH wave at 400 nm for the corresponding nanoantenna geometries (L = 110 nm (c), L = 150 nm (e), and L = 190 nm (g)).

followed by SERS, was shown to be inefficient for generating a strong enough signal to compete with the SEHRS signal.[30] The determination of the molecular hyperpolarizability is beyond the scope of the present work, but it is worth mentioning that numerical methods have been specifically developed for its computation, as density-functional theory and Hartree–Fock methods based on Taylor expansion of the hyperpolarizability

DOI: 10.1021/acs.jpcc.5b04128
J. Phys. Chem. C 2015, 119, 15547−15556

and perturbation method.[58−61] Here, we further neglect the tensorial nature of the hyperpolarizability and consider only the β_{xxx} component. The generalization to other tensor elements is straightforward. Furthermore, placing a molecular emitter at a specific spot within a plasmonic antenna is actually not necessary, because the field enhancement is much stronger in the gap of the antenna. Hence, even if molecules were spin-coated on the entire substrate, it is only those in the gap that will contribute to the experimental signal; this is especially the case for these experiments that use a nonlinear response of the system. The emitting dipole is given by[62]

$$p_x(\mathbf{r}, \omega_{\mathrm{HRS}}) = \beta_{xxx}(\omega_{\mathrm{HRS}}; \omega, \omega)E_x(\mathbf{r}, \omega)E_x(\mathbf{r}, \omega) \quad (1)$$

where $\mathbf{r}$ is the molecule position. Because we focus on low energy molecular vibrations, the HRS frequency is close to the second harmonic frequency ($\omega_{\mathrm{HRS}} \approx 2\omega$), the Raman shift being small. Using the reciprocity between far-field excitation and dipole emission,[40,56] the enhancement of the HRS emitted in the forward direction relative to that of a molecule in a homogeneous medium without nanostructure is given by the enhancement factor G_{SEHRS} defined as

$$G_{\mathrm{SEHRS}} = |E_x(\mathbf{r}, 2\omega)|^2 \cdot |E_x(\mathbf{r}, \omega)|^4 \quad (2)$$

where E_x denotes the ratio between the x-component of the electric field with and without the nanostructure at the position $\mathbf{r}$. The enhancement factor G_{SEHRS} has been evaluated for an incident wavelength λ = 800 nm, corresponding to an emitting wavelength λ = 400 nm, for a molecule located in the gap center of different DA (see Table 1). For comparison, the enhancement factor of the Raman scattering G_{SERS} is determined by

$$G_{\mathrm{SERS}} = |E_x(\mathbf{r}, \omega)|^4 \quad (3)$$

Table 1. Values of the Enhancement Factors G_{SEHRS} and G_{SERS} for a Molecule in the Gap of Al DA with Various Lengths

	arm length L (nm)		
	110	150	190
G_{SEHRS}	84 250	243 000	3030
G_{RS}	6240	22 500	10 800

The corresponding values are also reported in Table 1. Note that the factor G_{SERS} corresponds to the excitation stage of the factor G_{SEHRS}. Several important observations can be made from Table 1. First, a higher enhancement at the excitation stage does not necessary result in a higher enhancement factor G_{SEHRS} despite the nonlinear dependence. Indeed, a good enhancement at the excitation stage can be offset by a poor enhancement at the emission stage (L = 190 nm). Second, the enhancement factor G_{SEHRS} is 1 order of magnitude higher than the factor G_{RS} for L = 110 and 150 nm, but not for L = 190 nm, where it is actually about 3 times smaller than G_{SERS}. These two observations underline the importance of the electromagnetic properties of the plasmonic nanostructure at the emission step. This importance is further evidenced when looking at the emission patterns, red polar plots in Figure 2. For a fixed emission wavelength λ = 400 nm, the emission pattern of a dipole located at the gap center of a nanoantenna evolves with the length of the nanoantenna arms, from a dipole emission for L = 110 nm to a quadrupole emission for L = 190 nm, Figure 2b, d, and f. This evolution is due to the mode distribution at λ = 400 nm, where higher order modes can be excited for longer antennas (see the evolution of the near-field intensity in Figure 3).[63,64]

For low energy molecular vibrations, the strong incident laser light makes the direct observation of the weak SERS signal almost impossible. Indeed, suitable optical filters are required to reject the strong excitation laser to clearly observe Raman lines with a spectrometer. Contrary to RS, the hyper-Raman signal is far away from the pump wavelength; see Figure 1a. On the other hand, the wavelength of the hyper-Raman signal is close to the second harmonic wavelength for HRS involving low energy molecular vibrations, and the SHG from the plasmonic nanostructure could exceed the SEHRS signal.[65] Furthermore, the second harmonic intensity from the molecule is also related to its hyperpolarizability β. Hence, the SEHRS and the SHG signals from the molecule have nearly identical intensities, and this SHG cannot wipe out the SEHRS signal.[66] While the SHG from plasmonic structures is much weaker than the incident light,[67−69] it is also important to reduce the second harmonic intensity to increase the SEHRS visibility. To determine the relative properties of the SEHRS signal and the SHG from the plasmonic nanostructure, the SHG from the Al DA has been evaluated using a surface integral equation method,[45,46] and the corresponding emission patterns are shown as blue polar plots in Figure 2. Contrary to HRS, where the DA is driven by a dipole in the nanogap, SHG arises from the nanoantenna surface, where the centrosymmetry is broken.[47,48] The different physical origins for these two processes result in different emission patterns and near-field distributions; see Figures 2−4. Because of its symmetry properties, SHG always vanishes in the forward and backward directions, Figure 4, opening here two windows for the detection of the SEHRS signal in convenient directions that can be easily implemented experimentally.[70] Note that the second harmonic wave is described using even modes with respect to the origin of the system and the x-component of the second harmonic electric field vanishes in the (O, x, z) plane.[71] However, the enhancement factor G_{SEHRS} for the Al DA is much weaker than some of the factors G_{SERS} reported in the literature for various plasmonic nanostructures.[17] Indeed, the highest enhancement G_{SEHRS} for the Al DA is 2.5×10^5, while the factor G_{SERS} can be as high as 10^{10} for good SERS substrates.[15,16] It is therefore necessary to consider other plasmonic structures to increase the factor G_{SEHRS}.

To this end, because the wavelength of the HRS signal is close to the second harmonic wavelength for HRS involving low energy molecular vibrations, we investigate nanostructures that have been specifically designed to be resonant at both the fundamental wavelength (λ = 800 nm) and the second harmonic wavelength (λ = 400 nm). The DRA, a nanoantenna composed of three arms (two small arms and one long arm) and made of aluminum,[72] is a good example of such multiresonant nanostructures for nonlinear plasmonics, Figure 1c.[42] Following the previous approach developed for the Al DA, the intensity enhancement in the gaps when the DRA is driven by a planewave, and the enhancement of the dipole radiation has been evaluated using the SIE method, Figure 5 and Table 2. As expected, an enhancement of the intensity in both gaps is observed for wavelengths close to λ = 400 and 800 nm. Despite this fact, the enhancement factor G_{SEHRS} for the DRA is lower than that of the Al DAs with L = 110 or 150 nm because the dipolar resonance is large enough to be excited at 400 nm in the latter cases; compare Figure 2 with Figure 5. Furthermore, the

DOI: 10.1021/acs.jpcc.5b04128
J. Phys. Chem. C 2015, 119, 15547−15556

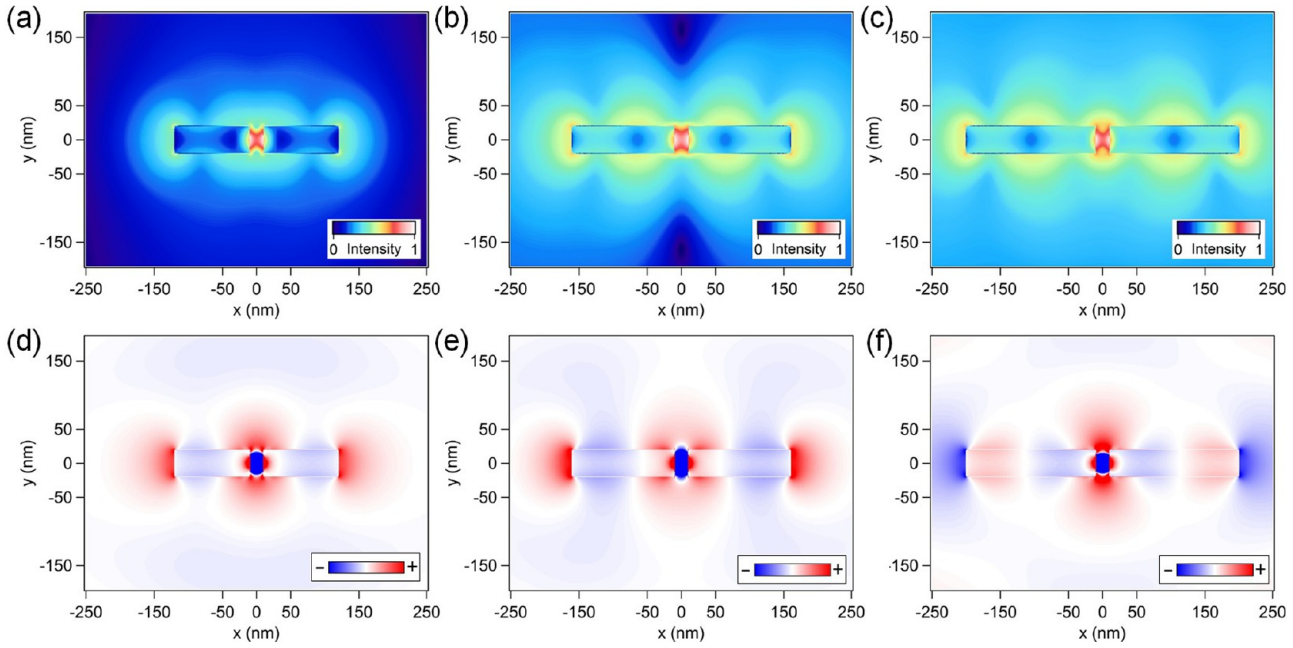

Figure 3. Near-field distribution of the electric field intensity close to Al dipolar nanoantennas driven by a dipole located at the gap center and polarized along the *x*-axis, for different arm lengths: (a) L = 110 nm, (b) L = 150 nm, and (c) L = 190 nm. The emission wavelength is λ = 400 nm. (d–f) The corresponding real part of the *x*-component of the electric field $Re(E_x)$ evaluated under the same conditions is also shown.

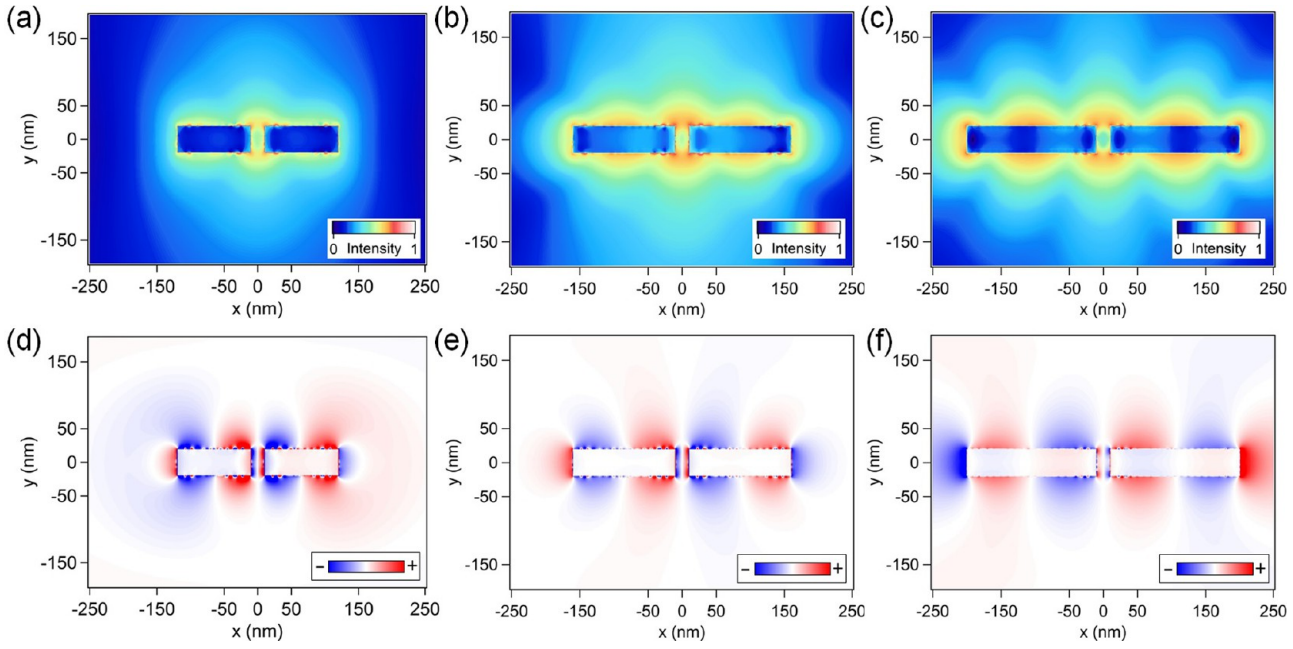

Figure 4. Near-field distribution of the SH electric field intensity close to Al dipolar nanoantennas for a SH wavelength λ = 400 nm (the calculations are performed for an excitation wavelength λ = 800 nm), for different arm lengths: (a) L = 110 nm, (b) L = 150 nm, and (c) L = 190 nm. (d–f) The corresponding real part of the *x*-component of the SH electric field $Re(E_x)$ evaluated under the same conditions is also shown.

second harmonic intensity, which is inclined to hide the HRS signal, is about 10 times higher for the DRA than for the DA; see Figure S1 in the Supporting Information. Figure 5 indicates that the asymmetry of the SHG does not open a window in the forward and backward directions for the DRA. Actually, the near-field distributions (Figure 6) of the SHG and of the dipole are very similar because the selection rules are broken in an asymmetric nanostructure. Because of all of these disadvantages, the DRA is not a plasmonic substrate of choice for SEHRS.

Recently, Fano resonances resulting from the coupling between a bright mode and dark mode have been used in nonlinear plasmonics to increase and control the fundamental near-field intensity;[73−76] they have also been used to enhance the Raman signal by taking advantage of their very strong near-field.[75] From the previous discussions about SEHRS with DA and DRA, it is clear that a good plasmonic substrate for SEHRS should be symmetric. For this reason, we consider now silver heptamers. The gaps between the silver nanoparticles are fixed to 10 nm for all of the gaps in the structure; all of the

DOI: 10.1021/acs.jpcc.5b04128
J. Phys. Chem. C 2015, 119, 15547−15556

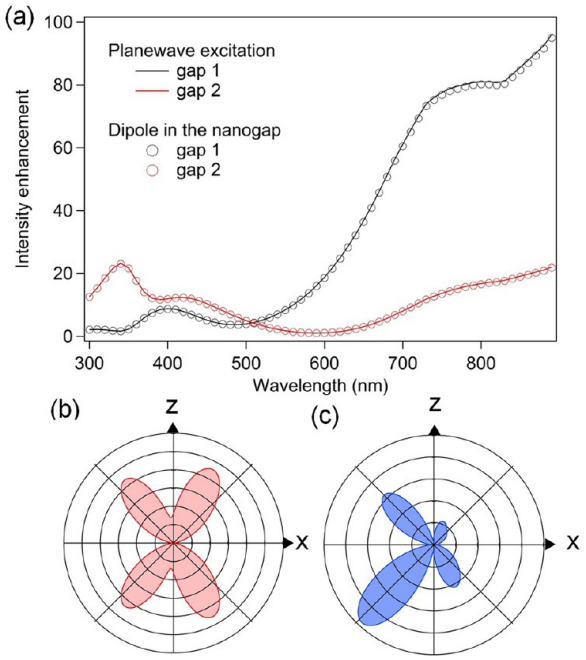

Figure 5. (a) Enhancement of the intensity in the two gaps of Al DRA (continuous lines) and enhancement of the radiation from a dipole located at one of the gap centers and polarized along the x-axis (dot). Gap 1 corresponds to the gap between the long rod and the central small rod, and gap 2 corresponds to the gap between the two small rods; see Figure 1c. In the case of the dipole radiation, the intensity is evaluated in the far-field region (at the point (0, 0, 50 μm)). (b) Emission pattern of a dipole located at the center of gap 1 (λ = 400 nm). (c) Emission pattern of the SH wave at λ = 400 nm for the DRA.

Table 2. Values of the Enhancement Factors G_{HRS} and G_{RS} for a Molecule in One of the Gaps of the DRA

	DRA	
	gap 1	gap 2
G_{SEHRS}	57 700	3360
G_{SERS}	6560	280

nanoparticles have the same diameter, which we vary between 70 and 120 nm. In the following, the field enhancement in two specific gaps is considered, which we denote as gap 1 and gap 2, Figure 1d. Gap 1 is one of the gaps between the three aligned silver nanodisks ($x > 0$ and $y = 0$), and gap 2 is the gap between the two silver nanodisks on the top of the heptamer ($x = 0$ and $y > 0$), Figure 1d. The intensity enhancements in the two other gaps are similar to those in gap 1 and gap 2, due to the symmetry properties of the heptamer, but not necessary equal. The backward scattered intensity reveals a Fano resonance with a dip position between λ = 600 and 820 nm, depending on the nanoparticles diameter, Figure 7a.[43,77] As expected, the excitation of the plasmonic dark mode induces a strong intensity enhancement in gaps 1 and 2, where it can exceed 2500× the incident intensity; see Figure 7b and Supporting Information Figure S2. The intensity enhancements in gaps 1 and 2 are different due to the interference between the bright mode and the dark mode resulting in the Fano resonance.[73] The enhancement factors G_{SEHRS} calculated for a molecule in gap 1 or 2 for the different disk diameters are reported in Table 3. The values obtained are several orders of magnitude higher (at least $\sim 10^3$) than those obtained for the DA and DRA (compare Tables 1 and 3); this underlines the benefit of plasmonic Fano resonances for molecular spectroscopy. As emphasized previously, the other key experimental point is the respective directivity of the second harmonic signal from the plasmonic nanostructure and that of the HRS signal from the studied molecule. The corresponding emission patterns are shown in Figure 7 for the Fano-resonant structure. In the case of a molecule in gap 1, the SEHRS emission pattern is always asymmetric due to the nonsymmetric excitation of the silver heptamers (Figure 8 and Supporting Information Figures S3,S4), and the SEHRS signal cannot be easily collected without SHG background. However, the HRS signal from a molecule in gap 2 is collimated along the z-axis (in the (O, x, z) plane), directions in which the second harmonic signal vanishes. This behavior is easily understood considering symmetry. Indeed, a dipole emitter excites odd-modes in the silver heptamers while SHG excites even-modes; compare Figure 8e with Figure 8f. Because the (O, x, z) and (O, y, z) planes are symmetry planes for the second harmonic electric field, the second harmonic intensity vanishes along the z-axis, opening there a window for the observation of the HRS signal with low SHG as was also the case for the DA. The SIE method can be used to compare the relative SHG between different plasmonic nanostructures. Here, we wish to make a quantitative comparison between the SHG from a heptamer and the SEHRS from a molecule interacting with that nanostructure. Hence, we need to determine the absolute hyperpolarizability of the silver heptamer expressed in esu. To this end, we performed SIE calculations for spherical 150 nm gold nanoparticles and used the corresponding experimental hyperpolarizability[78] $\beta = 1.1 \times 10^{-23}$ esu to deduct the heptamer hyperpolarizability. The experimental surface susceptibilities of gold and silver reported in ref 79 are used.[79] This way, we are able to report in Figure 9 simultaneously the SHG from the heptamer and the SEHRS for a molecule located in gap 2. As molecule we consider a donor−acceptor "push−pull" chromophore with a hyperpolarizability $\beta = 3 \times 10^{-27}$ esu.[80] The relative second harmonic and SEHRS signals shown in Figure 9 indicate that, although the maximal second harmonic intensity is 1 order of magnitude higher than the maximal HRS intensity, two windows with higher HRS intensity are clearly visible in the z-direction. Defining the limit of these windows as the angles for which the HRS and SHG intensities are equal, the window in the forward direction corresponds to a numerical aperture of 0.28, indicating that the two signals can be experimentally separated in confocal measurements. These results clearly point to an experimental configuration where SEHRS involving low energy molecular vibrations can be recorded with a low second harmonic background coming from the plasmonic substrate.

CONCLUSIONS

In summary, the design and the optimization of plasmonic substrates for SEHRS have been discussed. The two-photon excitation of the molecule was described using its hyperpolarizability β, and the emission of the hyper-Raman photons was reproduced using a dipole emitter located at the molecule position. Considering different geometries (including multiresonant antennas and silver heptamers supporting Fano resonances), the parameters influencing the enhancement of the HRS and its separation with the SHG from the plasmonics substrate have been investigated. The results reported in this Article emphasize the importance of optimizing the electromagnetic properties of the plasmonic substrate at both the

DOI: 10.1021/acs.jpcc.5b04128
J. Phys. Chem. C 2015, 119, 15547−15556

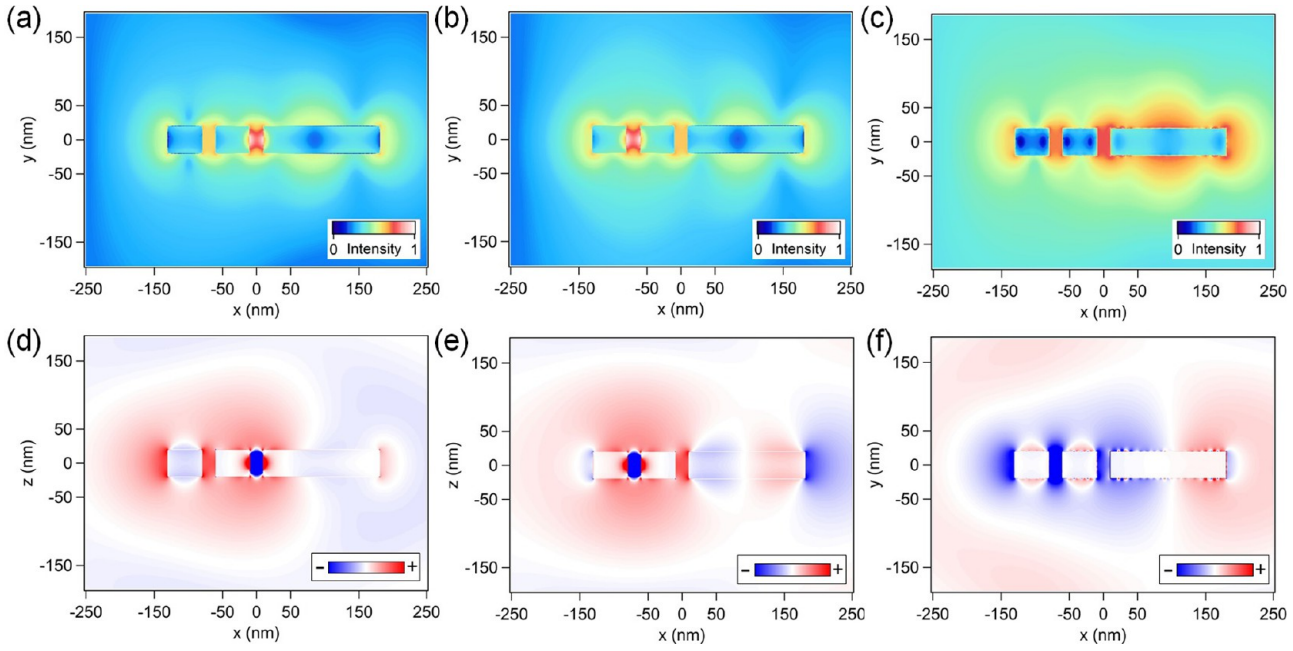

Figure 6. Near-field distribution of the electric field intensity close to the DRA driven by a dipole located (a) at the center of gap 1 and (b) at the center of gap 2. The emission wavelength is λ = 400 nm. (c) Near-field distribution of the SH intensity close to Al DRA for a SH wavelength λ = 400 nm. All of the dipoles are polarized along the x-direction. (d–f) Corresponding real parts of the x-component of the electric field $Re(E_x)$ evaluated under the same conditions.

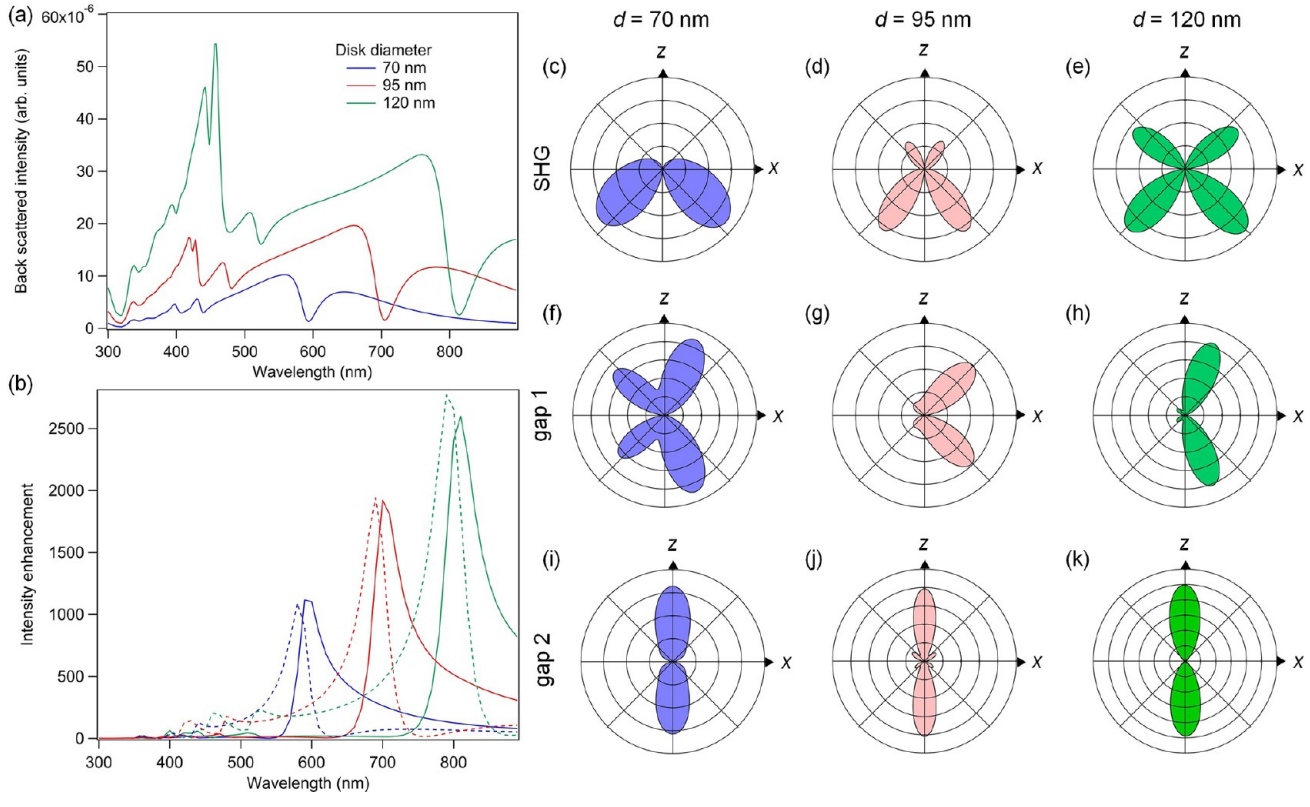

Figure 7. (a) Back scattered intensity and (b) intensity enhancement in gap 1 (full lines) and in gap 2 (dashed lines) as a function of the incident wavelength for a silver heptamer. The disk diameter is d = 70 nm (blue curves), d = 95 nm (red curves), and d = 110 nm (green curves). Emission patterns for the SH wave at λ = 400 nm for a silver heptamer with different disk diameters: (c) d = 70 nm, (d) d = 95 nm, (e) d = 120 nm. Emission patterns for a dipole polarized along the x-axis located at the center of the gap 1 (f, g, h) and gap 2 (i, j, k) for a silver heptamer with disk diameters of d = 70 nm (f, i), d = 95 nm (g, j), and d = 120 nm (h, k).

excitation and the emission wavelengths. This theoretical study paves the way for future experimental investigation of SEHRS. It is particularly important to extend surface-enhanced spectroscopy to SEHRS because some molecular vibrations

DOI: 10.1021/acs.jpcc.5b04128
J. Phys. Chem. C 2015, 119, 15547–15556

Table 3. Values of the Enhancement Factors G_{HRS} and G_{RS} for a Molecule in the Gap of a Silver Heptamer

	disk diameter (nm)					
	70		95		120	
gap:	1	2	1	2	1	2
G_{SEHRS}	695 200	22 450	1.6×10^6	28 600	3.6×10^8	2.1×10^8
G_{SERS}	15 800	4490	264 000	2600	5.7×10^6	7×10^6

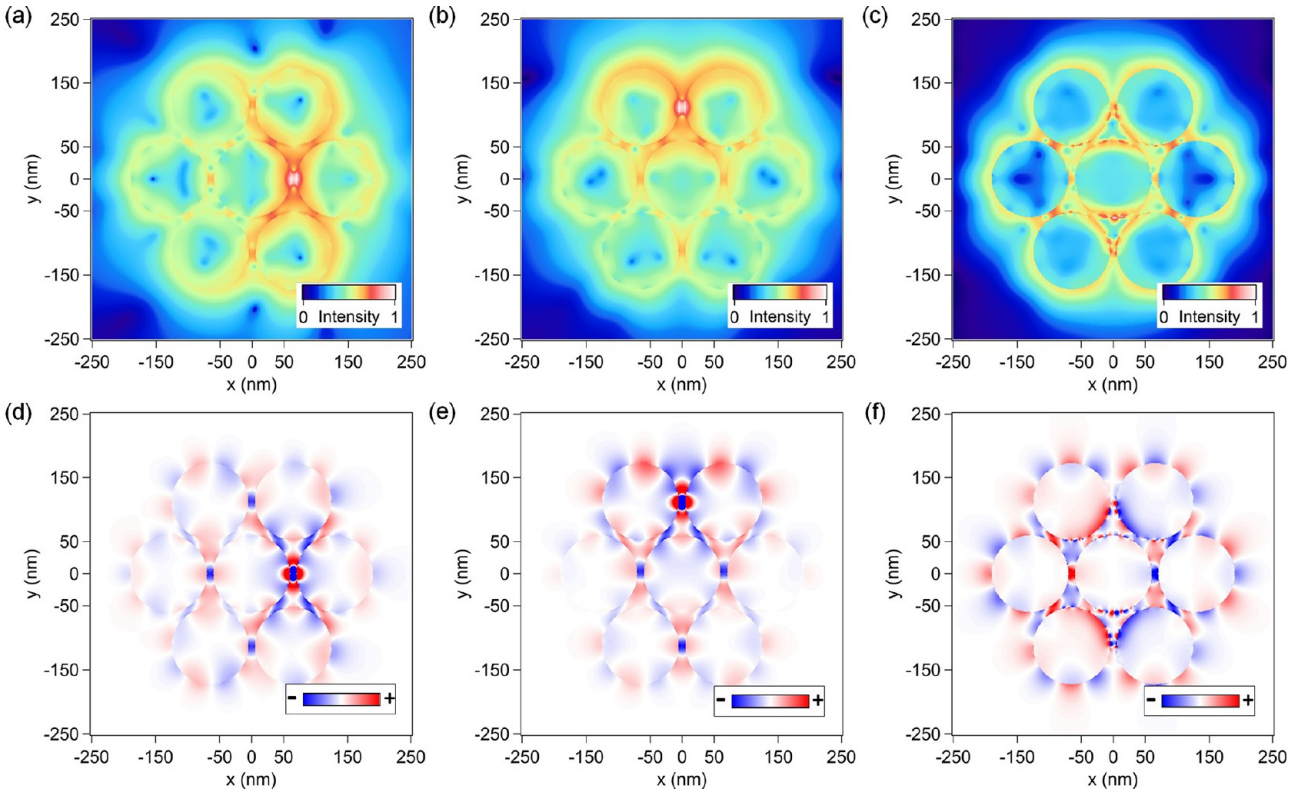

Figure 8. Near-field distribution of the electric field intensity close to silver heptamers driven by a dipole polarized along the x-axis and located (a) at the center of gap 1 and (b) at the center of gap 2. The emission wavelength is λ = 400 nm. The gap is fixed to 10 nm and the disk diameter is 120 nm. (c) Near-field distribution of the SH intensity close to the same silver heptamer for a SH wavelength λ = 400 nm. (d–f) Corresponding real part of the x-component of the electric field $Re(E_x)$ evaluated under the same conditions.

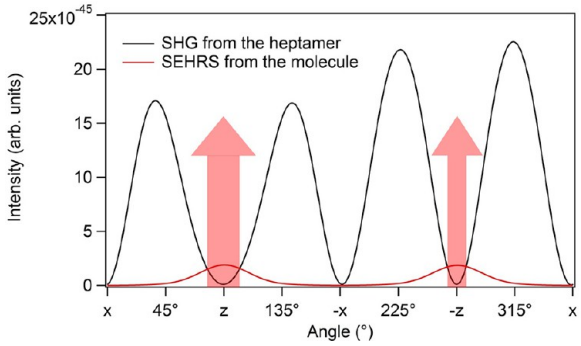

Figure 9. SHG from the silver heptamer with disk diameter d = 120 nm and SEHRS from a donor–acceptor "push–pull" chromophore with a hyperpolarizability of $\beta = 3 \times 10^{-27}$ esu located in gap 2. The two red arrows indicate the scattering angle ranges for which the HRS intensity is higher than the SHG intensity.

inactive in SERS and surface-enhanced infrared spectroscopy are active in SEHRS due to its different selection rules. The complementarity between SERS, surface-enhanced infrared spectroscopy, and SEHRS provides a unique possibility for characterizing the vibrational states and properties of single molecules. The method for rejecting the nonlinear signal from plasmonic substrate during surface-enhanced spectroscopy measurements presented in this Article is general and can be extended to other techniques, such as coherent anti-Stokes Raman spectroscopy, for example.[26,27]

■ ASSOCIATED CONTENT

Supporting Information

Comparison between the SHG from the dipole antenna and the double resonant antenna and additional computations performed for the silver heptamers. The Supporting Information is available free of charge on the ACS Publications website at DOI: 10.1021/acs.jpcc.5b04128.

■ AUTHOR INFORMATION

Corresponding Author

*E-mail: jeremy.butet@epfl.ch.

Notes

The authors declare no competing financial interest.

DOI: 10.1021/acs.jpcc.5b04128
J. Phys. Chem. C 2015, 119, 15547–15556

■ ACKNOWLEDGMENTS

Funding from the Swiss National Science Foundation (project 200020_153662) is gratefully acknowledged.

■ REFERENCES

(1) Hollas, J. M. *Modern Spectroscopy*; Wiley: Chichester, 2004.
(2) Moerner, W. E.; Fromm, D. P. Methods of Single-Molecule Fluorescence Spectroscopy and Microscopy. *Rev. Sci. Instrum.* **2003**, *74*, 3597.
(3) Kulzer, F.; Orrit, M. Single-Molecule Optics. *Annu. Rev. Phys. Chem.* **2004**, *55*, 585−611.
(4) Hildner, R.; Brinks, D.; Nieder, J. B.; Cogdell, R. J.; van Hulst, N. F. Quantum Coherent Energy Transfer over Varying Pathways in Single Light-Harvesting Complexes. *Science* **2013**, *340*, 1448−1451.
(5) Moskovits, M. Surface-Enhanced Spectroscopy. *Rev. Mod. Phys.* **1985**, *57*, 1783.
(6) Jackson, J. B.; Halas, N. J. Surface-Enhanced Raman Scattering on Tunable Plasmonic Nanoparticle Substrates. *Proc. Natl. Acad. Sci. U.S.A.* **2004**, *101*, 17930−17935.
(7) Talley, C. E.; Jackson, J. B.; Oubre, C.; Grady, N. K.; Hollars, C. W.; Lane, S. M.; Huser, T. R.; Nordlander, P.; Halas, N. J. Surface-Enhanced Raman Scattering from Individual Au Nanoparticles and Nanoparticle Dimer Substrates. *Nano Lett.* **2005**, *5*, 1569−1574.
(8) Zhang, W.; Fischer, H.; Schmid, T.; Zenobi, R.; Martin, O. J. F. Mode-Selective Surface-Enhanced Raman Spectroscopy Using Nanofabricated Plasmonic Dipole Antennas. *J. Phys. Chem. C* **2009**, *113*, 14672−14675.
(9) Willets, K. A.; Van Duyne, R. P. Localized Surface Plasmon Resonance Spectroscopy and Sensing. *Annu. Rev. Phys. Chem.* **2007**, *58*, 267−297.
(10) Lal, S.; Link, S.; Halas, N. J. Nano-Optics from Sensing to Waveguiding. *Nat. Photonics* **2007**, *1*, 641−648.
(11) Lakowicz, J. R. Radiative Decay Engineering: Biophysical and Biomedical Applications. *Anal. Biochem.* **2001**, *298*, 1−24.
(12) Osawa, M. Dynamic Processes in Electrochemical Reactions Studied by Surface-Enhanced Infrared Absorption Spectroscopy (SEIRAS). *Bull. Chem. Soc. Jpn.* **1997**, *70*, 2861−2880.
(13) Neubrech, F.; Pucci, A.; Cornelius, T. W.; Karim, S.; Garcia-Etxarri, A.; Aizpurua, J. Resonant Plasmonic and Vibrational Coupling in a Tailored Nanoantenna for Infrared Detection. *Phys. Rev. Lett.* **2008**, *101*, 157403.
(14) Maier, S. A. *Plasmonics: Fundamentals and Applications*; Springer: New York, 2007.
(15) Kneipp, K.; Wang, Y.; Kneipp, H.; Perelman, L. T.; Itzkan, I.; Dasari, R. R.; Feld, M. S. Single Molecule Detection Using Surface-Enhanced Raman Scattering (SERS). *Phys. Rev. Lett.* **1997**, *78*, 1667−1670.
(16) Nie, S.; Emory, S. R. Probing Single Molecules and Single Nanoparticles by Surface-Enhanced Raman Scattering. *Science* **1997**, *275*, 1102−1106.
(17) Le Ru, E. C.; Etchegoin, P. G. Single-Molecule Surface-Enhanced Raman Spectroscopy. *Annu. Rev. Phys. Chem.* **2012**, *63*, 65−87.
(18) Le Ru, E. C.; Etchegoin, P. G. *Principles of Surface-Enhanced Raman Spectroscopy and Related Plasmonic Effects*; Elsevier Science: Amsterdam, 2009.
(19) Wang, H.; Levin, C. S.; Halas, N. J. Nanosphere Arrays with Controlled Sub-10-nm Gaps as Surface-Enhanced Raman Spectroscopy Substrates. *J. Am. Chem. Soc.* **2005**, *127*, 14992−14993.
(20) Dieringer, J. A.; Lettan, R. B.; Scheidt, K. A.; Van Duyne, R. P. A Frequency Domain Existence Proof of Single-Molecule Surface-Enhanced Raman Spectroscopy. *J. Am. Chem. Soc.* **2007**, *129*, 16249−16256.
(21) Barhoumi, A.; Zhang, D.; Tam, F.; Halas, N. J. Surface-Enhanced Raman Spectroscopy of DNA. *J. Am. Chem. Soc.* **2008**, *130*, 5523−5529.
(22) Adato, R.; Altug, H. In-Situ Ultra-Sensitive Infrared Absorption Spectroscopy of Biomolecule Interactions in Real Time with Plasmonic Nanoantennas. *Nat. Commun.* **2013**, *4*, 2154.
(23) Brown, L. V.; Yang, X.; Zhao, K.; Zheng, B. Y.; Nordlander, P.; Halas, N. J. Fan-Shaped Gold Nanoantennas above Reflective Substrates for Surface-Enhanced Infrared Absorption (SEIRA). *Nano Lett.* **2015**, *15*, 1272−1280.
(24) Tolles, W. M.; Nibler, J. W.; McDonald, J. R.; Harvey, A. B. A Review of the Theory and Application of Coherent Anti-Stokes Raman Spectroscopy (CARS). *Appl. Spectrosc.* **1977**, *31*, 253−271.
(25) Evans, C. L.; Xie, X. S. Coherent Anti-Stokes Raman Scattering Microscopy: Chemical Imaging for Biology and Medicine. *Annu. Rev. Anal. Chem.* **2008**, *1*, 883−909.
(26) Zhang, Y.; Zhen, Y.-R.; Neumann, O.; Day, J. K.; Nordlander, P.; Halas, N. J. Coherent anti-Stokes Raman scattering with single-molecule sensitivity using a plasmonic Fano resonance. *Nat. Commun.* **2014**, *5*, 4424.
(27) Yamplosky, S.; Fishman, D. A.; Dey, S.; Hulkko, E.; Banik, M.; Potma, E. O.; Apkarian, V. A. Seeing a Single Molecule Vibrate Through Time-Resolved Coherent Anti-Stokes Raman Scattering. *Nat. Photonics* **2014**, *8*, 650−656.
(28) Kelley, A. M. Hyper-Raman Scattering by Molecular Vibrations. *Annu. Rev. Phys. Chem.* **2010**, *61*, 41−61.
(29) Golab, J. T.; Sprague, J. R.; Carron, K. T.; Schatz, G. C.; van Duyne, R. P. A Surface Enhanced Hyper-Raman Scattering Study of Pyridine Adsorbed Onto Silver: Experiment and Theory. *J. Chem. Phys.* **1988**, *88*, 7942−7951.
(30) Yang, W.-H.; Hulteen, J.; Schatz, G. C.; van Duyne, R. P. A Surface-Enhanced Hyper-Raman and Surface-Enhanced Raman Scattering Study of trans-1,2-bis(4-pyridyl)ethylene Adsorbed onto Silver Film over Nanosphere Electrodes. Vibrational Assignments: Experiment and Theory. *J. Chem. Phys.* **1996**, *104*, 4313−4323.
(31) Ikeda, K.; Takase, M.; Sawai, Y.; Nabika, H.; Murakoshi, K.; Uosaki, K. Hyper-Raman Scattering Enhanced by Anisotropic Dimer Plasmons on Artificial Nanostructures. *J. Chem. Phys.* **2007**, *127*, 111103.
(32) Cyvin, S. J.; Rauch, J. E.; Decius, J. C. Theory of Hyper-Raman Effects (Nonlinear Inelastic Light Scattering): Selection Rules and Depolarization Ratios for the Second-Order Polarizability. *J. Chem. Phys.* **1965**, *43*, 4083−4095.
(33) Ziegler, L. D. Hyper-Raman Spectroscopy. *J. Raman Spectrosc.* **1990**, *21*, 769−779.
(34) Kneipp, H.; Kneipp, K.; Seifert, F. Surface-Enhanced Hyper-Raman Scattering (SEHRS) and Surface-Enhanced Raman Scattering (SERS) by Means of Mode-Locked Ti:Sapphire Laser Excitation. *Chem. Phys. Lett.* **1993**, *212*, 374−378.
(35) Kneipp, K.; Kneipp, H.; Seifert, F. Near-Infrared Excitation Profile Study of Surface-Enhanced Hyper-Raman Scattering and Surface-Enhanced Raman Scattering by Means of Tunable Mode-Locked Ti: Sapphire Laser Excitation. *Chem. Phys. Lett.* **1995**, *233*, 519−524.
(36) Chu, Y.; Banaee, M. G.; Crozier, K. B. Double-Resonance Plasmon Substrates for Surface-Enhanced Raman Scattering with Enhancement at Excitation and Stokes Frequencies. *ACS Nano* **2010**, *4*, 2804−2810.
(37) Le, F.; Brandl, D. W.; Urzhumov, Y. A.; Wang, H.; Kundu, J.; Halas, N. J.; Aizpurua, J.; Nordlander, P. Metallic Nanoparticle Arrays: A Common Substrate for Both Surface-Enhanced Raman Scattering and Surface-Enhanced Infrared Absorption. *ACS Nano* **2008**, *2*, 707−718.
(38) Milojevich, C. B.; Mandrell, B. K.; Turley, H. K.; Iberi, V.; Best, M. D.; Camden, J. P. Surface Enhanced Hyper-Raman Scattering from Single Molecules. *J. Phys. Chem. Lett.* **2013**, *4*, 3420−3423.
(39) Kern, A. M.; Meixner, A. J.; Martin, O. J. F. Molecule-Dependent Plasmonic Enhancement of Fluorescence and Raman Scattering near Realistic Nanostructures. *ACS Nano* **2012**, *6*, 9828−9836.

DOI: 10.1021/acs.jpcc.5b04128
J. Phys. Chem. C 2015, 119, 15547−15556

(40) Kern, A. M.; Martin, O. J. F. Excitation and Reemission of Molecules near Realistic Plasmonic Nanostructures. *Nano Lett.* **2011**, *11*, 482−487.
(41) Kern, A. M.; Martin, O. J. F. Surface Integral Formulation for 3D Simulations of Plasmonic and High Permittivity Nanostructures. *J. Opt. Soc. Am. A* **2009**, *26*, 732−740.
(42) Thyagarajan, K.; Rivier, S.; Lovera, A.; Martin, O. J. F. Enhanced Second-Harmonic Generation from Double Resonant Plasmonic Antennae. *Opt. Express* **2012**, *20*, 12860−12865.
(43) Thyagarajan, K.; Butet, J.; Martin, O. J. F. Augmenting Second Harmonic Generation Using Fano Resonances in Plasmonic Systems. *Nano Lett.* **2013**, *13*, 1847−1851.
(44) Johnson, P. B.; Christy, R. W. Optical Constants of the Noble Metals. *Phys. Rev. B* **1972**, *6*, 4370−4379.
(45) Mäkitalo, J.; Suuriniemi, S.; Kauranen, M. Boundary Element Method for Surface Nonlinear Optics of Nanoparticles. *Opt. Express* **2011**, *19*, 23386−23399.
(46) Butet, J.; Gallinet, B.; Thyagarajan, K.; Martin, O. J. F. Second-Harmonic Generation from Periodic Arrays of Arbitrary Shape Plasmonic Nanostructures: a Surface Integral Approach. *J. Opt. Soc. Am. B* **2013**, *30*, 2970−2979.
(47) Wang, F. X.; Rodriguez, F. J.; Albers, W. M.; Ahorinta, R.; Sipe, J. E.; Kauranen, M. Surface and Bulk Contributions to the Second-Order Nonlinear Optical Response of a gold Film. *Phys. Rev. B* **2009**, *80*, 233402.
(48) Bachelier, G.; Butet, J.; Russier-Antoine, I.; Jonin, C.; Benichou, E.; Brevet, P.-F. Origin of Optical Second-Harmonic Generation in Spherical Gold Nanoparticles: Local Surface and Nonlocal Bulk Contributions. *Phys. Rev. B* **2010**, *82*, 235403.
(49) Heinz, T. F. Second-Order Nonlinear Optical Effects at Surfaces and Interfaces. In *Nonlinear Surface Electromagnetic Phenomena*; Ponath, H.-E., Stegeman, G. I., Eds.; Elsevier: Amsterdam, 1991.
(50) Lide, D. R. *CRC Handbook of Chemistry and Physics*; CRC Press: Boca Raton, FL, 2005.
(51) Girard, C.; Martin, O. J. F.; Dereux, A. Molecular Lifetime Changes Induced by Nanometer Scale Optical Fields. *Phys. Rev. Lett.* **1995**, *75*, 3098−3101.
(52) Huang, F. M.; Festy, F.; Richards, D. Tip-Enhanced Fluorescence Imaging of Quantum Dots. *Appl. Phys. Lett.* **2005**, *87*, 183101.
(53) Colas des Francs, G.; Girard, C.; Laroche, T.; Lévèque, G.; Martin, O. J. F. Theory of Molecular Excitation and Relaxation Near a Plasmonic Device. *J. Chem. Phys.* **2007**, *127*, 034701.
(54) Taminiau, T. H.; Stefani, F. D.; van Hulst, N. F. Enhanced Directional Excitation and Emission of Single Emitters by a Nano-Optical Yagi-Uda Antenna. *Opt. Express* **2008**, *16*, 16858−16866.
(55) Taminiau, T. H.; Stefani, F. D.; van Hulst, N. F. Optical Nanorod Antennas Modeled as Cavities for Dipolar Emitters: Evolution of Sub- and Super-Radiant Modes. *Nano Lett.* **2011**, *11*, 1020−1024.
(56) Curto, A. G.; Volpe, G.; Taminiau, T. H.; Kreuzer, M. P.; Quidant, R.; van Hulst, N. F. Unidirectional Emission of a Quantum Dot Coupled to a Nanoantenna. *Science* **2010**, *329*, 930−933.
(57) Le Ru, E. C.; Etchegoin, P. G. Rigorous Justification of the $|E|^4$ Enhancement Factor in Surface Enhanced Raman Spectroscopy. *Chem. Phys. Lett.* **2006**, *423*, 63−66.
(58) Neddersen, J. P.; Mounter, S. A.; Bostick, J. M.; Johnson, C. K. Nonresonant Hyper-Raman and Hyper-Rayleigh Scattering in Benzene and Pyridine. *J. Chem. Phys.* **1989**, *90*, 4719−4726.
(59) Quinet, O.; Champagne, B. Analytical Time-Dependent Hartree−Fock Schemes for the Evaluation of the Hyper-Raman Intensities. *J. Chem. Phys.* **2002**, *117*, 2481−2488.
(60) Quinet, O.; Champagne, B.; Rodriguez, V. Experimental and Theoretical Investigation of the Raman and Hyper-Raman Spectra of Acetonitrile and its Derivatives. *J. Chem. Phys.* **2006**, *124*, 244312.
(61) Ringholm, M.; Bast, R.; Oggioni, L.; Ekström, U.; Ruud, K. Analytic Calculations of Hyper-Raman Spectra from Density Functional Theory Hyperpolarizability Gradients. *J. Chem. Phys.* **2014**, *141*, 134107.
(62) Terhune, R. W.; Maker, P. D.; Savage, C. M. Measurements of Nonlinear Light Scattering. *Phys. Rev. Lett.* **1965**, *14*, 681−684.
(63) Hancu, I. M.; Curto, A. G.; Castro-Lopez, M.; Kuttge, M.; van Hulst, N. F. Multipolar Interference for Directed Light Emission. *Nano Lett.* **2014**, *14*, 166−171.
(64) Osberg, K. D.; Harris, N.; Ozel, T.; Ku, J. C.; Schatz, G. C.; Mirkin, C. A. Systematic Study of Antibonding Modes in Gold Nanorod Dimers and Trimers. *Nano Lett.* **2014**, *14*, 6949−6954.
(65) Kauranen, M.; Zayats, A. V. Nonlinear Plamonics. *Nat. Photonics* **2012**, *6*, 737−748.
(66) Kelley, A. M.; Leng, W.; Blanchard-Desce, M. Resonance Hyper-Raman Scattering from Conjugated Organic Donor−Acceptor "Push−Pull" Chromophores with Large First Hyperpolarizabilities. *J. Am. Chem. Soc.* **2003**, *125*, 10520−10521.
(67) Butet, J.; Duboisset, J.; Bachelier, G.; Russier-Antoine, I.; Benichou, E.; Jonin, C.; Brevet, P.-F. Optical Second Harmonic Generation of Single Metallic Nanoparticles Embedded in a Homogeneous Medium. *Nano Lett.* **2010**, *10*, 1717−1721.
(68) Zhang, Y.; Grady, N. K.; Ayala-Orozco, C.; Halas, N. J. Three-Dimensional Nanostructures as Highly Efficient Generators of Second Harmonic Light. *Nano Lett.* **2011**, *11*, 5519−5523.
(69) Bautista, G.; Huttunen, M. J.; Mäkitalo, J.; Kontio, J. M.; Simonen, J.; Kauranen, M. Second-Harmonic Generation Imaging of Metal Nano-Objects with Cylindrical Vector Beams. *Nano Lett.* **2012**, *12*, 3207−3212.
(70) Dadap, J. I.; Shan, J.; Eisenthal, K. B.; Heinz, T. F. Second-Harmonic Rayleigh Scattering from a Sphere of Centrosymmetric Material. *Phys. Rev. Lett.* **1999**, *83*, 4045−4048.
(71) Butet, J.; Dutta-Gupta, S.; Martin, O. J. F. Surface Second-Harmonic Generation from Coupled Spherical Plasmonic Nanoparticles: Eigenmode Analysis and Symmetry Properties. *Phys. Rev. B* **2014**, *89*, 245449.
(72) Knight, M. W.; King, N. S.; Liu, L.; Everitt, H. O.; Nordlander, P.; Halas, N. J. Aluminum for Plasmonics. *Nano Lett.* **2014**, *14*, 834−840.
(73) Luk'yanchuck, B.; Zheludev, N. I.; Maier, S. A.; Halas, N. J.; Nordlander, P.; Giessen, H.; Chong, C. T. The Fano Resonance in Plasmonic Nanostructures and Metamaterials. *Nat. Mater.* **2010**, *9*, 707−715.
(74) Verellen, N.; Sonnefraud, Y.; Sobhani, H.; Hao, F.; Moshchalkov, V. V.; Van Dorpe, P.; Nordlander, P.; Maier, S. A. Fano Resonances in Individual Coherent Plasmonic Nanocavities. *Nano Lett.* **2009**, *9*, 1663−1667.
(75) Ye, J.; Wen, F.; Sobhani, H.; Lassiter, J. B.; Van Dorpe, P.; Nordlander, P.; Halas, N. J. Plasmonic Nanoclusters: Near Field Properties of the Fano Resonance Interrogated with SERS. *Nano Lett.* **2012**, *12*, 1660−1667.
(76) Gallinet, B.; Martin, O. J. F. Influence of Electromagnetic Interactions on the Line Shape of Plasmonic Fano Resonances. *ACS Nano* **2011**, *5*, 8999−9008.
(77) Hentschel, M.; Saliba, M.; Vogelgesang, R.; Giessen, H.; Alivisatos, A. P.; Liu, N. Transition from Isolated to Collective Modes in Plasmonic Oligomers. *Nano Lett.* **2010**, *10*, 2721−2726.
(78) Russier-Antoine, I.; Benichou, E.; Bachelier, G.; Jonin, C.; Brevet, P.-F. Multipolar Contributions of the Second Harmonic Generation from Silver and Gold Nanoparticles. *J. Phys. Chem. C* **2007**, *111*, 9044−9048.
(79) Krause, D.; Teplin, C. W.; Rogers, C. T. Optical Surface Second Harmonic Measurements of Isotropic Thin-Film Metals: Gold, Silver, Copper, Aluminum, and Tantalum. *J. Appl. Phys.* **2004**, *96*, 3626.
(80) Alain, V.; Thouin, L.; Blanchard-Desce, M.; Gubler, U.; Bosshard, C.; Günter, P.; Muller, J.; Fort, A.; Barzoukas, M. Molecular Engineering of Push−Pull Phenylpolyenes for Nonlinear Optics: Improved Solubility, Stability, and Nonlinearities. *Adv. Mater.* **1999**, *11*, 1210−1214.

DOI: 10.1021/acs.jpcc.5b04128
J. Phys. Chem. C 2015, 119, 15547−15556